PCCP

Investigation of field effects in the solid-state nanopore transistor

Journal:	*Physical Chemistry Chemical Physics*
Manuscript ID	CP-ART-05-2015-003125.R2
Article Type:	Paper
Date Submitted by the Author:	23-Sep-2015
Complete List of Authors:	Youn, Yong; Seoul National University, Department of Materials Science and Engineering Han, Seungwu; Seoul National University, Department of Materials Science and Engineering

PCCP

RSCPublishing

ARTICLE

Investigation of field effects in the solid-state nanopore transistor

Cite this: DOI: 10.1039/x0xx00000x

Yong Youn[a] and Seungwu Han*[a]

Received 00th January 2012,
Accepted 00th January 2012

DOI: 10.1039/x0xx00000x

www.rsc.org/

In order to calculate ion currents through solid-state nanopore transistors realistically, we propose a computational model based on the Poisson-Nernst-Plank equation. In the present model, we determine the surface charge density *locally* on the nanopore by imposing consistency between the ion distribution and chemical reaction at the surface. The model can consider a non-uniform influence by the gate voltage on the inner surface of the nanopore membrane, which enables us to investigate ion currents depending on the gate geometry such as thickness and vertical position within the nanopore. We verify the validity of the model by comparing the pH dependence of simulation results with extant experimental results. We also investigate the transistor behaviour depending on the surface material, pore geometry and gate position. In particular, we propose an optimized system to enhance the on/off ratio of the nanopore transistor.

Introduction

Nanopores have been used in various applications, notably in DNA sequencing[1-6] and bio-sensing[7-10]. Since the dimension of nanopore is comparable to the Debye length in solution, the ion distribution and ion transport through the nanopore depend on the surface charge density on the nanopore wall. For example, it is known that pH condition or ion concentration affect the charge density on the nanopore wall,[11-15] which in turn slows down the translocation speed of DNA.[5, 16-18]

Recently, it has been proposed that the surface charge density can be electrically controlled by embedding the gate electrode inside the solid-state nanopore, reminiscent of the metal-oxide-semiconductor field-effect transistor (MOSFET) in microelectronic devices.[19-27] In the solid-state nanopore transistor, the gate potential affects the electric-double layer (EDL) by modifying charge groups on the surface as well as nearby ion concentration. The nanopore transistor has advantages that it can control the ionic transport precisely and instantaneously. Furthermore, in combination with the ionic diode,[28-30] it can manipulate, switch, redirect, and amplify the signal, realizing full-blown ionic circuits that mimic the electronic counterparts.[21] Several experiments demonstrated the usefulness of the nanopore transistor.[25, 26] For example, in ref. 25, the translocation speed of DNA was reduced by 20 folds in the "off" state of the transistor. Furthermore, the capture rate of DNA was also enhanced.[26] However, more dramatic improvements are in demand for detecting individual base pairs.

The computational modeling is the favored method in understanding the working principle of nanopore transistor as well as designing a promising device structure. So far, various theoretical models[31-37] have been suggested to understand the gate effect in the nanopore. However, each model has certain limitations that originate from the underlying approximations. For instance, the modulation of surface charge density was neglected in ref. 31-34. More recent models consider the variation of the surface charge density with respect to the gate voltage[35-37]. However, they still treat the gate effect within the one-dimensional model and so neglect the non-uniformity of surface potential on the inner wall, which becomes significant when the gate electrode is thinner than the nanopore membrane. Furthermore, the models calculate the potential distribution within EDL by the Grahame equation that precludes overlapping EDLs. This compromises the computational accuracy when the thickness of EDL is larger than the pore radius.

In this study, we develop a numerical model of the nanopore transistor that explicitly considers the finite thickness of the gate electrode within the nanopore membrane. The present model calculates the potential distribution in the membrane based on the Poisson-Nernst-Planck (PNP) model.[38-40] The surface charge density is determined by imposing self-consistency among the ion distribution near the surface and the chemical reaction of surface hydroxyl groups.[41, 42] Using the proposed computational model, we investigate the transistor behavior depending on the surface material, pore geometry and gate position. Based on the results, we propose a way to enhance the on/off ratio of the nanopore transistor by modifying the gate geometry.

Model

As a model system, we assume a cylindrical nanopore transistor where the gate electrode is embedded and surface is covered by oxide. Fig. 1 shows the material structure and simulation domains of the typical gate-embedded conical nanopore transistor. The boundary conditions in PNP equation are compiled in table 1 for each boundary numbered in the figure. Since the dimension of reservoir is sufficiently large, ions do not flow along the radial direction on boundary 2 and 8, resulting in the no-flux and zero-charge boundary conditions.[38-40] In the present model, electric potentials within not only electrolyte but also membrane (dielectric films and oxides) are explicitly computed. On the other hand, the Nernst-Plank equation is the governing equation in solution that produce ion distribution and flow. We impose the axial symmetry and solve PNP equation on the 2-dimensional space.

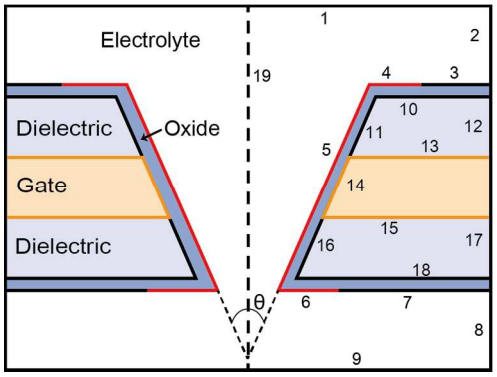

Fig. 1 Schematic of the nanopore used for PNP model. The sketch illustrates the electrolyte, oxide material, dielectric films, charged surface of the membrane (red, surface 4-6), gate/membrane interface (orange, surface 13-15) and axial symmetry line (dashed line, surface 19). The pore angle (θ) is also defined.

Table 1 Boundary conditions for governing equations

Surface	Nernst-Planck equation	Poisson equation
1	Concentration, $c_i = c_0$	Electric potential, $V = V_D (= -1\ \mathrm{V})$
2, 3, 7, 8	No flux, $-\mathbf{n}\cdot\mathbf{N}_i = 0$	Zero charge, $\mathbf{n}\cdot\mathbf{D} = 0$
4-6	No flux, $-\mathbf{n}\cdot\mathbf{N}_i = 0$	Surface charge, $\mathbf{n}\cdot(\mathbf{D}_1 - \mathbf{D}_2) = \sigma$
9	Concentration, $c_i = c_0$	Ground, $V = 0$
19	Axial symmetry	Axial symmetry
13-16		Electric potential, $V = V_G$
10-12, 16-18		Zero charge, $\mathbf{n}\cdot\mathbf{D} = 0$

c_i: ion concentration of the i^{th} ionic species; c_0: bulk concentration; $\mathbf{n}$: vector normal to the surface; $\mathbf{N}_i$: ionic flux of the ith ionic species; V_D: drain potential; $\mathbf{D}$: Electric displacement field; σ: surface charge density; V_G: gate potential

The reactive groups on the oxide surface is in chemical equilibrium with solution, which dictates their charge states. Here we assume that the hydroxyl group is a sole reactive group on the surface and it undergoes the following chemical reactions:[41-45]

$$\mathrm{R\cdot OH} \leftrightarrow \mathrm{R\cdot O^- + H^+} \quad (1)$$

$$\mathrm{R\cdot OH_2^+} \leftrightarrow \mathrm{R\cdot OH + H^+}, \quad (2)$$

where R indicates the metal atom in the oxide surface. The surface charge density (σ_{chem}) at the specific position of $\mathbf{r}_s$ on the surface is given by

$$\sigma_{\mathrm{chem}}(\mathbf{r}_s) = e\Gamma^{\mathrm{OH_2^+}}(\mathbf{r}_s) - e\Gamma^{\mathrm{O^-}}(\mathbf{r}_s) \quad (3)$$

where $\Gamma^{\mathrm{OH_2^+}}(\mathbf{r}_s)$ and $\Gamma^{\mathrm{O^-}}(\mathbf{r}_s)$ are the density of $\mathrm{OH_2^+}$ and $\mathrm{O^-}$ groups at $\mathbf{r}_s$ on the surface, respectively, and e is the electron charge (positive). Since the density of reactive groups (Γ) is roughly constant over the surface, the following relation holds:

$$\Gamma = \Gamma^{\mathrm{OH_2^+}}(\mathbf{r}_s) + \Gamma^{\mathrm{OH}}(\mathbf{r}_s) + \Gamma^{\mathrm{O^-}}(\mathbf{r}_s). \quad (4)$$

With $\mathrm{p}K_1$ and $\mathrm{p}K_2$ as equilibrium constants corresponding to the chemical reaction in eq. (1) and eq. (2), respectively, the ratios of charged reactive groups satisfy the following mass-action laws:

$$10^{-\mathrm{p}K_1} = \frac{[\mathrm{H^+}]_s \Gamma^{\mathrm{O^-}}}{\Gamma^{\mathrm{OH}}} \quad (5)$$

$$10^{-\mathrm{p}K_2} = \frac{[\mathrm{H^+}]_s \Gamma^{\mathrm{OH}}}{\Gamma^{\mathrm{OH_2^+}}}, \quad (6)$$

where $[\mathrm{H^+}]_s$ indicates hydrogen activity close to $\mathbf{r}_s$. From eq. (3)-(6), σ_{chem} relate to $[\mathrm{H^+}]_s$ as follows:

$$\sigma_{\mathrm{chem}} = e\Gamma\left[\left(1 + \frac{10^{-\mathrm{p}K_2}}{[\mathrm{H^+}]_s} + \frac{10^{-\mathrm{p}K_1}10^{-\mathrm{p}K_2}}{[\mathrm{H^+}]_s[\mathrm{H^+}]_s}\right)^{-1} - \left(1 + \frac{[\mathrm{H^+}]_s}{10^{-\mathrm{p}K_1}} + \frac{[\mathrm{H^+}]_s[\mathrm{H^+}]_s}{10^{-\mathrm{p}K_1}10^{-\mathrm{p}K_2}}\right)^{-1}\right] \quad (7)$$

On the other hand, the ratio between $[\mathrm{H^+}]_s$ and $[\mathrm{H^+}]_0$, the hydrogen activity in the bulk solution, is the same as that between $(c_+)_s$ and

$(c_+)_0$, the corresponding cation concentrations because they lie in the same electrostatic potential. That is to say,

$$[H^+]_s = \frac{[H^+]_0 (c_+)_s}{(c_+)_0} = \frac{10^{-pH} (c_+)_s}{(c_+)_0} \quad . \tag{8}$$

It is evident that eq. (7) and (8) are related self-consistently; for the given $\sigma^{in}_{chem}(\mathbf{r}_s)$, the PNP model brings forth $(c_+)_s$. Then, $[H^+]_s$ is obtained through eq. (8), which in turn gives $\sigma^{out}_{chem}(\mathbf{r}_s)$ from eq. (7). $\sigma^{out}_{chem}(\mathbf{r}_s)$ should match with $\sigma^{in}_{chem}(\mathbf{r}_s)$, leading to the self-consistency condition. We recall that σ_{chem}, $[H^+]_s$, and $(c_+)_s$ are all local functions that depend on $\mathbf{r}_s$. The self-consistency cycle determine $\sigma_{chem}(\mathbf{r}_s)$ together with the ion current flowing through the nanopore transistor.

Results and Discussions

In this section, we present computational results on the ion current of the nanopore transistor based on the theoretical model proposed in the previous section. We employ the COMSOL Multiphysics program throughout this study. The ion concentration is set to 0.1 mM KCl and we fix some geometrical parameters for the convenience of comparison; narrow diameter of the pore (20 nm), pore length (500 nm), thickness of gate electrode (100 nm), and thickness of oxide layer (5 nm). The diffusion coefficient of K^+ and Cl^- are $1.95\times10^{-9}\,m^2/s$ and $2.03\times10^{-9}\,m^2/s$, respectively. The applied source-drain voltage is −1 V, i.e., K^+ flows from the bottom to top reservoirs. We applied a wide range of gate voltages, from -3 to 3 V, to show the influence of the gate potential clearly. The maximum electric field in our simulation is comparable to the typical dielectric strength of oxides. Therefore, the comparison with experiment should be made on the smaller voltage range. The channel dielectric materials are SiO_2 or Al_2O_3 that are widely used in experiment. pK_1/pK_2 values of SiO_2 and Al_2O_3 are 7.5/−2[42-44] and 9.5/4.4[41], respectively. Density of chemical reaction groups of SiO_2 and Al_2O_3 are assumed to be 8×10^{-18} m^{-2}.[35]

pH dependence

In order to check the validity of the present model, we first reproduce pH dependence of ion current in the nanopore transistor, which was examined in refs. 20, 25, and 45. In experiment, either monotonic[20] or unipolar[45] behaviour was found when the gate potential changes the sign. (The dielectric material was SiO_2 in both experiments.) The difference originates from the pH condition of the solution. Fig. 2 shows the computed ion current versus gate voltage of the straight nanopore transistor in different pH conditions of 5 and 7. We recall that SiO_2 surface is negatively charged in both pH 5 and 7 solutions. Since it is negatively charged, the concentration of positive ions inside the pore is much higher than that of negative ions, and so the number of positive ions is a critical parameter governing the ion current. This also results in the p-type behaviour.

The inset figures in Fig. 2 show the positive ion concentration inside the pore. The ion current is modulated according to the gate voltage. When the negative gate potential is applied, the number of K^+ around gate increases, resulting in the larger ion current in both pH conditions. In contrast, the positive gate reduces the K^+ concentration around the gate region and hence the ionic current.

In Fig. 2, the off state is observed only in the pH 5 condition where the oxide surface is negatively charged in small amounts under the zero gate potential. In this case, the concentration of K^+ ions screening the surface charge is also small. The positive gate potential then easily repels K^+ ions from the nanopore, reducing ion currents close to zero. On the other hand, if the oxide surface is more negatively charged as in pH 7 solution, K^+ ions still remain around the gate in spite of the positive gate, and the off state is not achieved. These results are consistent with the experiment; in the acidic solution, unipolar behaviour is observed and the ion current shows a monotonic behaviour under pH 7 condition.

To examine the influence of ion concentrations, we compare results under two different ion concentrations, 0.1 and 1 mM in Fig. S1 in the supplementary material. It is clear that transistor-like behavior is maintained even in the higher KCl concentration. However, on/off ratio in the 0.1 mM condition is larger than that in the 1 mM condition. This is because in the low ion concentration, EDL related to the ion concentration inside the pore becomes thicker so the influence of gate potential becomes larger.

In passing, we compare the present model with the prefixed surface charge model on the typical transistor-like behaviour in Fig. 2a. The results are shown in Fig. S2 in the supplementary material. In the prefixed model, a bipolar behavior was found, which is not consistent with experimental results. This indicates that the variation of surface charge is critical for realistic simulations.

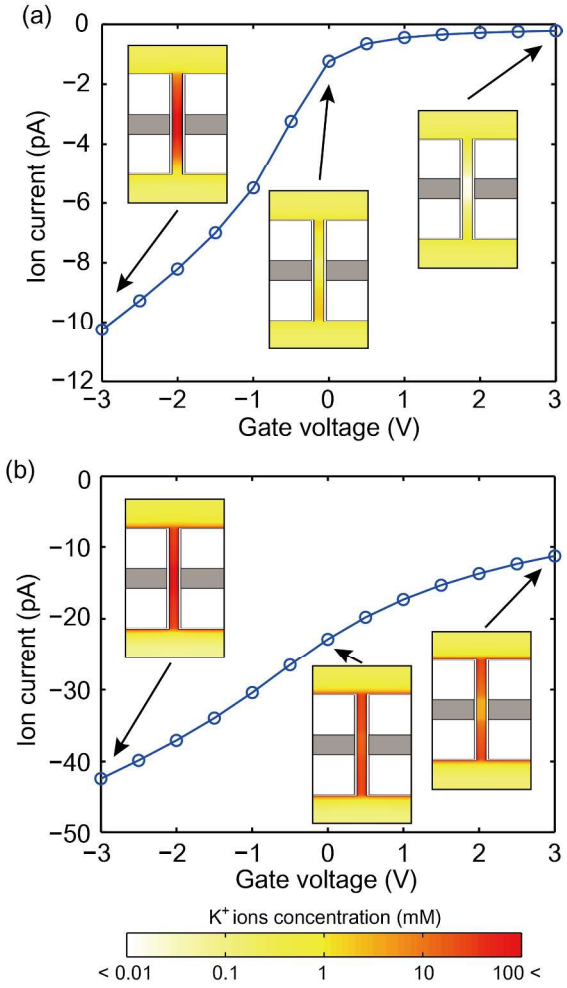

Fig. 2 Ion current versus gate voltage in (a) pH 5, (b) pH 7 condition. Inset figures show the K^+ ion distribution. The gate electrode inside the nanopore membrane is shown as shaded regions.

Effect of oxide materials

Next, we compare the p-type transistor behaviour and related properties depending on the oxide material covering the nanopore. This part was motivated by recent experiments showing that the ion current responds differently to the gate voltage depending on the material for gate oxides.[34, 45, 46] In the previous studies,[47] σ_{chem} under zero gate potential was used in explaining the material dependence. However, the gate-induced modulation in σ_{chem} should be also included because it also affects the response of the ion current significantly. In order to show the effect of gate oxide, we consider SiO_2 and Al_2O_3 that are widely used in experiments. To compare fairly the influence of gate potential, we adjust the pH value such that surface charge densities on both oxides are the same under the zero gate potential. This is achieved with pH values of 5 and 7.6 for SiO_2 and Al_2O_3, respectively.

Fig. 3a shows the ion currents as a function of the gate voltage when SiO_2 and Al_2O_3 cover the nanopore. It is seen that the ion current in Al_2O_3 is less sensitive to modulation of the gate voltage than that in SiO_2. These behaviours can be explained from the response of surface potential and σ_{chem} to the gate voltage as shown in Fig. 3b and 3c. In Fig. 3b, the surface potential of Al_2O_3 changes within a narrow range in comparison with SiO_2, which results in the limited response as shown in Fig. 3a.

Several factors such as gate voltage, dielectric constant of oxide, and chemical groups affect the surface potential. From the detailed analysis, we find that the modulation of σ_{chem} is the dominant factor in the present case. In Fig. 3c, it is seen that σ_{chem} in Al_2O_3 changes linearly and more widely than SiO_2. According to Eq. (7), pK and pH values determine the sign and magnitude of the surface charge. The pK_1 (9.5) and pK_2 (4.4) values of Al_2O_3 are relatively close to the pH value (7.5), indicating that surface reactive groups readily assume positive or negative charges in response to the gate potential. The facile variation of σ_{chem} on Al_2O_3 can effectively screen the gate potential, weakening its influence on the ion distribution. In contrast, SiO_2 surface can be only negatively charged in the given pH condition due to the large difference between pK_2 (-2) and pH condition (5), resulting in the non-linear behaviour of σ_{chem}. The present results demonstrate that the current-voltage characteristics of nanopore transistors can be controlled by selecting gate oxides with proper pK values.

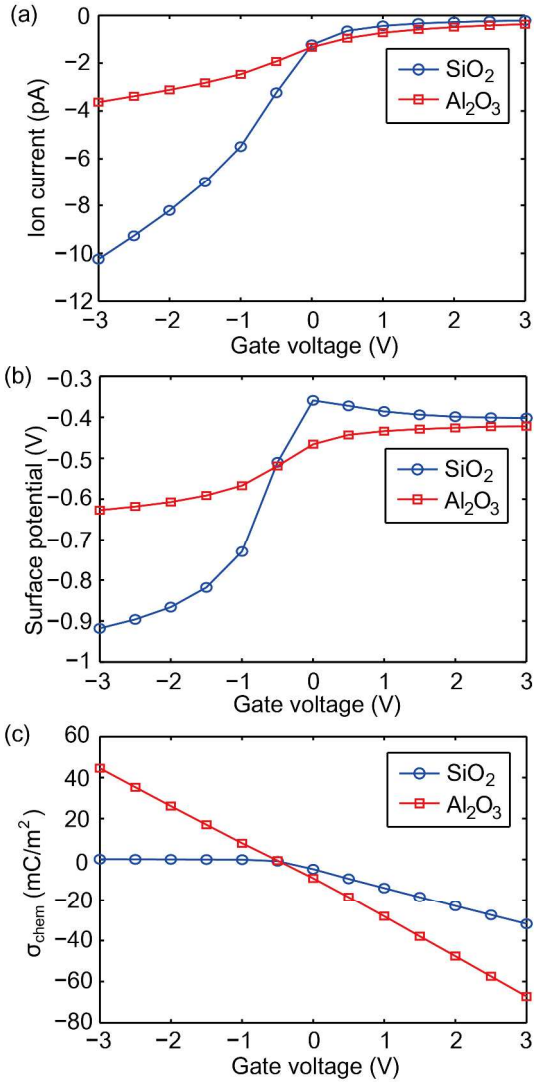

Fig. 3 (a) Ion current, (b) surface potential, and (c) surface charge density (σ_{chem}) with respect to the gate voltage for SiO_2 and Al_2O_3. Surface charge density and potential at surface are calculated at the middle position of the gate electrode.

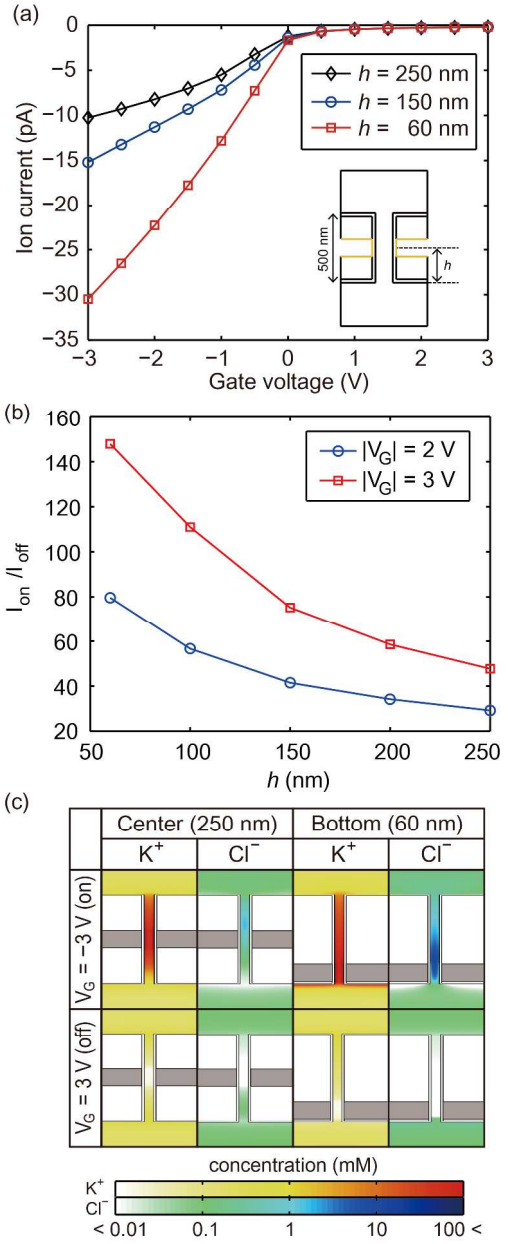

Fig. 4 (a) Ion current versus gate voltage depending on the position of gate electrode. The inset shows the position of gate electrode. (b) The on/off ratio with respect to the gate position when the magnitude of gate potential is 2 or 3 V. (c) Ion distribution depending on the gate potential and position of gate electrode. The gate electrode inside the nanopore membrane is shown as shaded regions.

Influence of device geometry

In this subsection, we study on transistor-like behaviour depending on the device geometry. Specifically, we try to maximize the on/off ratio, a critical device parameter as a transistor, by changing the position of the gate electrode and the pore angle. We limit the simulation condition to pH 5 solution and SiO_2 as the oxide layer. First, we show in Fig. 4a current versus gate voltage depending on the position of gate electrode. When the position of the gate electrode moves from the middle of the membrane (h = 250 nm) to near the outer membrane at the bottom (h = 60 nm), the on current increases while the off current decreases, enhancing the on/off ratio monotonically, as can be seen in Fig. 4b.

To explain the dependence on the gate position in the above, we analyze the ion concentration inside the pore. Fig. 4c shows colour maps for the K^+ and Cl^- concentrations on a plane perpendicular to the membrane for gate voltages of ±3 V and center/bottom gate positions. When the gate electrode is placed in the middle of the membrane, gate potential only affects the ion distribution inside the pore. If the gate position is lowered from 250 to 60 nm, the gate potential affects the salt concentration on broader regions including the pore entrances,

in particular at the bottom. This is because the gate electrode influences the potential of electrolyte near the bottom side of the membrane. Since the negative drain potential pulls K^+ ions from the bottom to the top reservoir, the on current increases. The on/off ratio is further enhanced by reducing the K^+ ions near the pore entrance under the positive gate potential. Therefore, the gate electrode placed near the lower side of the membrane produces larger on/off ratios. On the other hand, when the gate electrode is placed near the top side of the membrane, we find that the on/off ratio is reduced than for the middle position, which can be easily understood from the foregoing discussions.

Next, to further enhance on/off ratio, we modify the pore angle of nanopore (θ) while the gate electrode is fixed at the bottom region (see Fig. 1). The gate dependent ion currents are shown in Fig. 5a. In contrast to the gate position in the above, increasing the pore angle does not lead to the monotonous change in on/off ratio as shown in the inset, and the on/off ratio peaks at a specific angle.

When the pore angle opens up, both on and off currents increase and so the on/off ratio varies depending on the relative increase rate. In the low-angle region (θ < 6°), the increase of the on current is larger than that of the off current, which can be understood by the ion distribution shown in Fig. 5b in the case of straight pore (θ = 0°). When the pore angle is small, it is difficult for ions to pass through the narrow pore under the positive gate potential, which hinders the enhancement of the off current. Thus, the on/off ratio increases as the pore angle becomes bigger. As the pore angle exceeds the optimal value, however, the increase of the number of ions moving through the pore under the off state is larger than that under the on state, leading to the decrease of on/off ratio. Consequently, the on/off ratio peaked at around 6°.

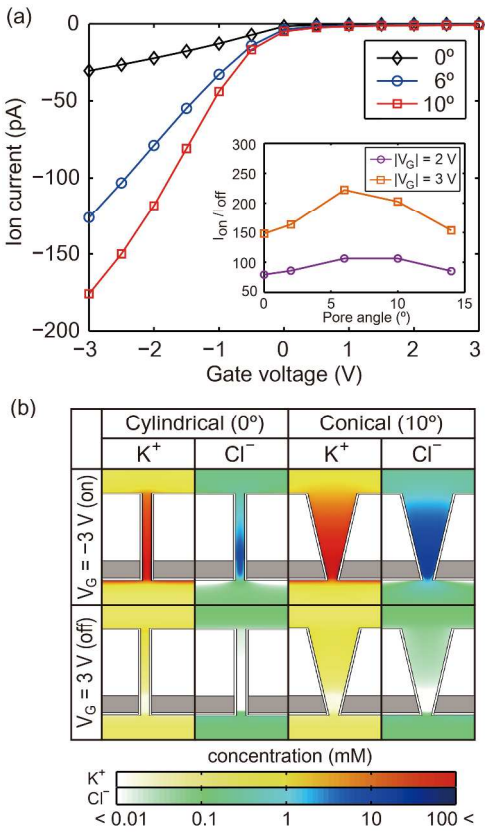

Fig. 5 (a) Ion current vs. gate voltage depending on the pore angle. Inset in (a) is the on/off ratio with respect to the pore angle when the magnitude of gate potential is 2 or 3 V. (b) Ion distribution depending on the gate potential and pore angle. The gate electrode inside the nanopore membrane is shown as shaded regions.

Conclusion

In summary, we proposed a computational model to simulate the effect of gate potential in a gate-embedded nanopores. The main improvement over the previous works is that the present model calculates the surface charge density locally, extending its applicability to wide range of nanopore transistors. By solving the model numerically, we showed that the unipolar behaviour is observed in the SiO_2 surface at the pH 5 condition. In addition, by comparing the response of ion current in the different gate oxides, we demonstrated that that the current-voltage characteristics of nanopore transistors can be controlled by selecting gate oxides with proper pK values. We also optimized the geometry such as gate position and pore angle, to maximize on/off current ratios. Our results showed that geometric effect and chemical reaction can be tuned to control transistor-like behaviour of the ion current. We believe that the present model can be widely used in the research of the nanopore transistor.

Acknowledgements

We thank Prof. Wonmuk Hwang for helpful discussions. This work was supported by the Pioneer Research Center Program

through the National Research Foundation of Korea funded by the Ministry of Education, Science and Technology (2012-0009563). The computations were carried out at KISTI (No. KSC-2014-C3-012).

Notes and references

[a] Department of materials Science and Engineering and Research Institute of Advanced Materials, Seoul National University, Seoul 151-744, Korea.

† Footnotes should appear here. These might include comments relevant to but not central to the matter under discussion, limited experimental and spectral data, and crystallographic data.

Electronic Supplementary Information (ESI) available: [details of any supplementary information available should be included here]. See DOI: 10.1039/b000000x/

1 V. Dimitrov, U. Mirsaidov, D. Wang, T. Sorsch, W. Mansfield, J. Miner, F. Klemens, R. Cirelli, S. Yemenicioglu, and G. Timp, *Nanotechnology*, 2010, **21**, 065502

2 B. M. Venkatesan, B. Dorvel, S. Yemenicioglu, N. Watkins, I. Petro, and R. Bashir, *Adv. Mater.*, 2009, **21**, 2771-2776

3 J. Li, M. Gershow, D. Stein, E. Brandin, and J. A. Golovchenko, *Nature Mater.*, 2003, **2**, 611-615

4 P. Chen, E. Brandin, Y. R. Kim, Q. Wang, and D. Branton, *Nano Lett.*, 2004, **4**, 2293-2298

5 R. M. M. Smeets, U. F. Keyser, D. Krapf, M. Y. Wu, N. H. Dekker, and C. Dekker, *Nano Lett.*, 2006, **6**, 89-95

6 A. J. Storm, J. H. Chen, H. W. Zandbergen, and C. Dekker, *Phys. Rev. E*, 2005, **71**, 051903

7 S. Howorka and Z. Siwy, *Chem. Soc. Rev.*, 2009, **38**, 2360-2384

8 C. Dekker, *Nature Nanotechnol.*, 2007, **2**, 209-215

9 A. J. Haes, S. Zou, G. C. Schatz, and R. P. Van Duyne, *J. Phys. Chem. B*, 2004, **108**, 109-116

10 J. D. Uram, K. Ke, A. J. Hunt, and M. Mayer, *small*, 2006, **2**, 967-972

11 W. Guo, Y. Tian and L. Jiang, *Acc. Chem. Res.*, 2013, **46**, 2834-2846

12 W. Guo, L. Cao, J. Xia, F. -Q. Nie, W. Ma, J. Xue, Y. Song, D. Zhu, Y. Wang and L. Jiang, *Adv. Funct. Mater.*, 2010, **20**, 1339

13 J. Gao, W. Guo, D. Feng, H. Wang, D. Zhao and L. Jiang, *J. Am. Chem. Soc.*, 2014, **136**, 12265-12272

14 L. Cao, W. Guo, Y. Wang, L. Jiang, *Langmuir*, 2012, **28**, 2194-2199

15 L. Cao, W. Guo, W. Ma, L. Wang, F. Xia, S. Wang, Y. Wang, L. Jiang and D. Zhu, *Energy Environ. Sci.*, 2011, **4**, 2259-2266

16 D. Fologea, M. Gershow, B. Ledden, D. S. McNabb, J. A. Golovchenko, and J. Li, *Nano Lett.*, 2005, **5**, 1905-1909

17 B. N. Anderson, M. Muthukumar, and A. Meller, *ACS Nano*, 2013, **7**, 1408-1414

18 D. Fologea, J. Uplinger, B. Thomas, D. S. McNabb, and J. Li, *Nano Lett.*, 2005, **5**, 1734-1737

19 N. Hu, Y. Ai, and S. Qian, *Sens. Actuators B*, 2012, **161**, 1150-1167

20 R. Karnik, R. Fan, M. Yue, D.Y. Li, P.D. Yang, and A. Majumdar, *Nano Lett.*, 2005, **5**, 943-948

21 S. Mafe, J. A. Manzanares, and P. Ramirez, *J. Phys. Chem. C*, 2010, **114**, 21287-21290

22 S. -W. Nam, M. J. Rooks, K. -B. Kim, and S. M. Rossnage, *Nano Lett.*, 2009, **9**, 2044-2048

23 Y. He, M. Tsutsui, C. Fan, M. Taniguchi, and T. Kawai, *ACS Nano*, 2011, **5**, 5509-5518

24 E. B. Kalman, O. Sudre, I. Vlassiouk, and Z. S. Siwy, *Anal. Bioanal. Chem.*, 2009, **394**, 413-419

25 P. -c. Yen, C. -h. Wang, G. -J. Hwang, and Y. C. Chou, *Rev. Sci. Instrum.*, 2012, **83**, 034301

26 K. -H. Paik, Y. Liu, V. Tabard-Cossa, M. J. Waugh, D. E. Huber, J. Provine, R. T. Howe, R. W. Dutton and R. W. Davis, *ACS Nano*, 2012, **6**, 6767-6775

27 S. Wu, F. Wildhaber, A. Bertsch, J. Brugger, and P. Renaud, *Appl. Phys. Lett.*, 2013, **102**, 213108

28 L. -J. Cheng and L. J. Guo, *Chem. Soc. Rev.*, 2010, **39**, 923-938

29 I. Vlassiouk and Z. S. Siwy, *Nano Lett.*, 2007, **7**, 552-556

30 R. Yan, W. Liang, R. Fan, and P. Yang, *Nano Lett.*, 2009, **9**, 3820-3825

31 K. P. Singh and M. Kumar, *Lab Chip*, 2012, **12**, 1332-1339

32 Y. Ai, J. Liu, B. Zhang, and S. Qian, *Sens. Actuators B*, 2011, **157**, 742-751

33 A. Nikolaev and M. E. Gracheva, *J. Comput. Electron*, 2014, **13**, 818-825

34 S. -H. Lee, H. Lee, T. Jin, S. Park, B. J. Yoon, G. Y. Sung, K. -B. Kim, and S. J. Kim, *Nanoscale*, 2015, **7**, 936-946

35 Z. Jiang and D. Stein, *Langmuir*, 2010, **26**, 8161-8173

36 Z. Jiang and D. Stein, *Phys. Rev. E*, 2011, **83**, 031203

37 S. Xue, L. -H. Yeh, Y. Ma, and S. Qian, *J. Phys. Chem. C*, 2014, **118**, 6090-6099

38 J. Cervera, B. Schiedt, R. Neumann, S. Mafe(é), and P. Ramirez, *J. Chem. Phys.*, 2006, **124**, 104706

39 R. B. Schoch, J. Han, and P. Renaud, *Rev. Mod. Phys.*, 2008, **80**, 839-883

40 D. Constantin and Z. S. Siwy, *Phys. Rev. E*, 2007, **76**, 041202

41 Z. Todorovic and S. K. Milojic, *J. Serb. Chem. Soc.*, 2004, **69**, 1063-1072

42 N. Sahai and D. A. Sverjensky, *Geochim. Cosmochim. Acta*, 1997, **61**, 2801-2826

43 S. H. Behrens and D. G. Grier, J. Chem. Phys., 2001, 115, 6716-6712

44 X. Liu, J. Cheng, X. Lu, and R. Wang, *Phys. Chem. Chem. Phys.*, 2014, **16**, 26909-26916

45 J. Bai, D. Wang, S. -w. Nam, H. Peng, R. Bruce, L. Gignac, M. Brink, E. Kratschmer, S. Rossnagel, P. Waggoner, K. Reuter, C. Wang, Y. Astier, V. Balagurusamy, B. Luan, Y. Kwark, E. Joseph, M. Guillorn, S. Polonsky, A. Royyuru, S. P. Rao, and G. Stolovitzky, *Nanoscale*, 2014, **6**, 8900-8906

46 S. -W. Nam, M. -H. Lee, S. -H. Lee, D. -J. Lee, S. M. Rossnagel, and K. -B. Kim, *Nano Lett.*, 2010, **10**, 3324-3329

47 A. Uddin, S. Yemenicioglu, C. -H. Chen, E. Corigliano, K. Milaninia and L. Theogarajan, Nanotechnology, 2013, **24**, 155501